STING1 activation in brain endothelium by *Plasmodium*-sequestered heme leads to lethal cerebral malaria through activation of type I IFN response.

Teresa Faria Pais[1*], Hajrabibi Ali[1], Joana Moreira da Silva[1, 2], Nádia Duarte[1], Rita Neres[1], Chintan Chhatbar[3, 4], Rita C. Acúrcio[5], Rita C. Guedes[5], Maria Carolina Strano Moraes[6], Bruno Costa Silva[6], Ulrich Kalinke[3] and Carlos Penha-Gonçalves[1,7*]

1- Instituto Gulbenkian de Ciência, Oeiras, Portugal

2- CIISA, Faculdade de Medicina Veterinária, Universidade de Lisboa, Portugal

3- Institute for Experimental Infection Research, TWINCORE, Centre for Experimental and Clinical Infection Research, a joint venture between the Helmholtz Centre for Infection Research and the Hannover Medical School, Hannover, Germany.

4- Institute of Neuropathology, Medical Faculty, University of Freiburg, Freiburg, Germany.

5- Research Institute for Medicines (iMed.ULisboa), Faculty of Pharmacy, Universidade de Lisboa, Portugal.

6- Systems Oncology Group, Champalimaud Research, Champalimaud Centre for the Unknown, Lisbon, Portugal

7- Lead contact

* Correspondence: mtpais@igc.gulbenkian.pt; cpenha@igc.gulbenkian.pt;

Abstract

Cerebral malaria (CM), caused by infection with *Plasmodium falciparum*, is characterized by brain inflammation. Type I IFN inflammatory response underlies CM pathogenesis leading to brain endothelium dysfunction with the loss of blood-brain-barrier (BBB). We identified the stimulator of interferon response cGAMP interactor 1 (STING1) as the key innate immune sensor that activates type I IFN pathway and CXCL10 expression governing brain leukocyte infiltration and CM lethality in mice. Brain endothelial-specific IFNβ-reporter and STING1 KO mice unveiled a critical role of brain endothelial cells (BECs) in fuelling type I IFN-driven inflammation in the brain during malaria infection. We show that extracellular particles (EPs) derived from *Plasmodium*-infected erythrocytes and containing digestive vacuoles trigger a STING1-dependent IFNβ response in BECs. This response increases with heme content in digestive vacuoles, which directly activates BECs via STING1. Together, our findings uncovered that heme-stimulated endothelial STING1 drives type I IFN response and subsequent brain pathology.

Introduction

Malaria, the disease caused by Plasmodium infection, accounted for 409 000 deaths worldwide in 2019, a drawback in the WHO global strategy to control malaria (World Malaria Report 2019). Despite malarial treatment, children under 5 years of age can develop cerebral malaria (CM) upon infection with *Plasmodium falciparum*, facing the highest risk of malaria morbidity and mortality (15-20%) (1). Brain swelling with increased compression of respiration centers in the brain stem predicts a fatal CM outcome (2,3). Even children who survive CM may develop cognitive and speech impairments due to long-term neurological sequelae (1).

Infected erythrocytes (IE), parasite components released during the blood-stage infection (e.g. malarial hemozoin and labile heme), and systemic inflammatory factors (eg. CXCL10, TNF, IL1β and IFNγ) elicit an unfettered brain endothelial cell response. Consequently, the brain endothelium function becomes compromised (reviewed in (4)), losing its BBB functions and allowing leaking of plasma proteins and water into the cerebral parenchyma that results in intracranial hypertension (reviewed in (5)). However, whether brain endothelial cells (BECs) are bystander activated by systemic inflammatory factors or are the source of brain inflammation and pathology remains largely unexplored in CM.

Over the last years, the type I interferons IFNα and IFNβ emerged as key mediators in innate immune responses to malaria, promoting brain immunopathology (reviewed in (6)). While this pathway was associated with protective immunity in children with uncomplicated malaria (7,8), polymorphism in regulatory regions of type I IFN receptor (IFNAR1 subunit) gene associated with increased type I IFN signaling linked to the development of CM in children (2) though other IFNAR gene variants were associated with reduced risk of CM (3,4).

In the experimental mouse model of CM, despite the protective role of type I IFN in early infection (9,10), several reports show that ablation of IFNAR1 signaling prevents BBB disruption and pathogenesis of experimental CM driven by parasite-specific cytotoxic $CD8^+$ T cells (11,12). In addition, mice deficient in type I IFN signaling molecules, i.e., KO for the transcription factors interferon regulatory factor 3 (IRF3) and 7 (IRF7) and the upstream TAK-binding kinase 1 (TBK1), are protected from CM (13). Moreover, a point mutation in the ubiquitin-specific protease 15 (USP 15) deters the type I IFN signature in the mouse brain and dampens brain inflammation increasing mice survival to CM (14). Accordingly, IFNAR blockade with a monoclonal antibody at later stages of *Plasmodium* infection decreases neurological signs and death in infected mice (8).

Several pattern recognition receptors (PRRs) underlie inflammatory responses during *Plasmodium* infection by binding to *Plasmodium*-derived components (15), such as GPI anchors, plasmodial DNA and RNA, and hemozoin, a byproduct of hemoglobin digested by the parasite, consisting of crystals made of polymerized heme (16). Moreover, labile heme generated as a byproduct of hemolysis during *Plasmodium* infection can also signal via PRR (17) and has also been shown to contribute critically to the pathogenesis of CM (18,19).

The cGAS-STING1 pathway, a major sensor of cytosolic DNA, recognizes AT-rich motifs in plasmodial DNA inducing IFN-β transcription in human monocytes and mouse macrophages (13,20,21). Interestingly, extracellular vesicles derived from *Plasmodium*-IE (20) and complexes of plasmodial DNA with hemozoin (22) were postulated as possible carriers of parasite DNA delivered into the cytosol of human monocytes.

In the brain, endothelial cells can capture malarial antigens that are cross-presented to parasite-specific $CD8^+$ T cells (23). Malarial antigens can be delivered to the endosomal and cytosolic compartments of endothelial cells either by parasitized-erythrocytes through fusion with membrane of endothelial cells or by uptake of merozoites and digestive vacuoles (23,24).

Ubiquitous expression of type I IFN and IFNAR1 poses a significant challenge to the identification of specific cellular and molecular contributions of type I IFN signaling activation in CM. Although BECs are within the first cells to sense the IE, their innate type I IFN-mediated innate immune response during CM remains to be elucidated. Here, we identified the STING1 activation in the brain, particularly in BECs, as a molecular mechanism involved in the detection of heme containing IE-derived particles underlying the pathogenesis of CM.

Material and Methods

Animals and treatment

All procedures involving laboratory mice were in accordance with national (Portaria 1005/92) and European regulations (European Directive 86/609/CEE) on animal experimentation and were approved by the Instituto Gulbenkian de Ciência Ethics Committee and the Direcção-Geral de Alimentação e Veterinária, the national authority for animal welfare.

Mice were housed and bred in the facilities of Instituto Gulbenkian de Ciência (Suppl. Table 1). *Myd88*$^{-/-}$ (MyD88 KO) mice were originally a gift from Prof. Shizuo Akira (Osaka University). *Mda5*$^{-/-}$mice were obtained from Dr. Maria Mota (IMM, Portugal). Transgenic mice expressing Cre under the GFAP promoter (GFAPCre) in C57BL/6 background were obtained from Dr. Henrique Veiga Fernandes (Champalimaud Foundation, Portugal).

Ifnβ1$^{-/-}$ (IFNβ KO), *Ifnβ1*$^{+/\Delta\beta\text{-luc}}$ (IFNβ-reporter mice), *Ifnβ1*$^{\text{flox}\beta\text{-luc/flox}\beta\text{-luc}}$ (IFNβ $^{\text{flox}\beta\text{-luc/flox}\beta\text{-luc}}$), *Trif*$^{-/-}$ (TRIF KO), B6(Cg)-*Tmem173*$^{tm1.2Camb}$/J (*Tmem173*$^{-/-}$, STING1 KO), Tg(Slco1c1-icre/ERT2)1Mrks (Slco1c1CreERT2) and *Myd88*$^{-/-}$*Trif*$^{-/-}$*Mavs*$^{-/-}$*Sting1*$^{-/-}$ (MyTrMaSt KO) mice were obtained from the TWINCORE, Centre for Experimental and Clinical Infection Research, Hanover, Germany.

C57BL/6J, B6;129-*Mavs*^{tm1Zjc}/J (MAVS KO), B6;SJL-*Sting1*$^{tm1.1Camb}$/J (STING1$^{\text{flox/flox}}$) , B6.Cg-Tg(Tek-cre)1Ywa/J (Tie2Cre), B6J.B6N(Cg)-*Cx3cr1*$^{tm1.1(cre)Jung}$/J (CX3CR1Cre), B6.129P2(Cg)-*Cx3cr1*$^{tm2.1(cre/ERT2)Litt}$/*WganJ* (CX3CR1CreERT2) and B6.129P2-*Lyz2*$^{tm1(cre)Ifo}$/*J* mice (LysMCre) were originally purchased from The Jackson Laboratory (Bar Harbor, ME) (Table S1). MAVS KO mice were backcrossed to C57BL/6J mice up to 96.82% of recipient genome. IFNβ$^{\text{flox}\beta\text{-luc/flox}\beta\text{-luc}}$ and STING1$^{\text{flox/flox}}$ were crossed with the different Cre lines to generate cell lineage conditional IFNβ-reporter, IFNβ KO mice

or STING1 KO mice. Experimental animals carrying one loxP-flanked and one KO allele of *Sting1* were generated by crossing Slco1c1Cre^{ERT2}STING1$^{flox/flox}$ or CX3CR1Cre^{ERT2} STING1$^{flox/flox}$ mice with STING1 KO mice. The efficiency of the conditional *Sting1* deletion was expected to be improved by having just one floxed allele. Crossing of STING1$^{flox/flox}$ mice with CX3CR1CreSTING1$^{+/+}$ or Tie2Cre STING1$^{+/+}$ mice generated a deleted loxP-flanking Sting1 allele in the germ line. These mice were then crossed with STING1$^{flox/flox}$ and originated Cre^{+} mice with one deleted *Sting1* allele while another allele remained loxP-flanked and was conditionally deleted. Mice with either a deletion of the floxed allele or a KO allele but also expressing a floxed *Sting1* allele were designated STING1$^{flox/-}$.

Wild type, deleted and floxed alleles of *Ifnβ1* and *Sting1* were identified in experimental animals by genotyping using a 3-primer strategy (Suppl. Table 2). For induction of *Sting1* deletion, 4-6 week old male and female mice were treated with tamoxifen (2 mg/10 g body weight) in corn oil administered by gavage every other day, totaling five doses. Mice were allowed to recover from tamoxifen treatment for 4 weeks.

For *in vivo* labelling of proliferating cells, mice received four intraperitoneal injections of BrdU (50 mg/kg,) every two hours. Brains were collected for FACS analysis two hours after the last injection and intracardiac perfusion of the mice with PBS.

As a positive control for luciferase activity in IFNβ-reporter mice in GFAP^{+} cells, mice received an intraperitoneal injection (i.p.) of 0.4 mg of Poly I:C.

Parasites and infection

Mice were infected with 10^6 IE with the following parasite strains: *Plasmodium berghei* ANKA (*Pba*) or *Pba*-GFP (25) to induce CM or with *Pb* NK65, a strain that proliferates in mice but does not induce neurological signs of CM.

Frozen IE stocks were expanded in C57BL/6 mice prior to infection. Parasitemia in mice infected with non-GFP parasites (*Pba* and *Pb* NK65) and GFP-*Pba* was determined by flow cytometry analysis as the percentage of DRAQ5^{+} erythrocytes (blood samples incubated with DRAQ5™, 3 uM) and GFP^{+} erythrocytes, respectively (LSRFortessa™ X-20 cell analyser, BD Biosciences and FACSDiVa software version 6.2).

Evaluation of CM

Neurological score

Wild-type mice developed severe signs of CM such as head deviation, paralysis, and convulsions at days 6–7 post infection (PI) and died within 4–6 h of severe disease development. In different genetic backgrounds death by CM occurred up to 11 days PI ("CM time window"). Mice resistant to CM died around day 20 with hyperparasitemia (~60%) without signs of severe neurological dysfunction.

Disease severity was evaluated in mice before and after infection following an adapted health score for CM (26). From day 4 PI mice were scored based on eleven parameters: gait/body posture, grooming, motor performance, balance, hindlimb clasping reflex, limb strength, toe pinch, aggressiveness, head deviation, paralysis and convulsions. For each parameter a maximum score of two was given to good response or health condition (normal gait, full body extension, clean and sheen hair, exploring of 3-4 corners in 30 sec, extending front feet on the wall of the cage, normal plantar reaction, active pull away, toe pinch reaction, normal aggressiveness, no convulsions, no paralysis or no head deviation). Clear signs of CM (convulsions, paralysis and head deviation) with no strength, no balance and no toe pinch reaction scored zero. Healthy mice scored 22 and mice dying of CM could score between 3-16 points at day 6 PI.

Blood–brain barrier integrity assay

At day 6 PI, when C57BL/6J wild type mice show signs of CM, the different mouse groups were killed 1 hour after retro-orbital injection of 100 μl of 2% Evans blue (EB) dye (Sigma) and were perfused intracardially with 15 ml of PBS. Brains were dissected, weighed, and pictured. EB retained in the brain tissue was extracted by immersion in 2 ml formamide (Merck) at 37°C in the dark for 48 h, and measured by spectrophotometry at 620 and 740 nm (Thermo Scientific™ Multiskan™ GO Microplate Spectrophotometer). Amounts of EB were calculated using an EB standard and expressed as mg EB/g of brain tissue.

Immune cells analysis

Spleen (day 5 PI) and brain (day 6 PI) single cell suspensions of infected and non-infected C57BL/6J and KO mice were immuno-stained for T cell and monocyte/macrophage activation cell surface markers. Brain single-cell suspensions were prepared as described before (27). Briefly, mice were perfused with 20 ml of PBS via the left ventricle of the heart. Brains were removed and homogenized in HBSS containing collagenase VIII (0.2 mg/ml) (Sigma). After incubation for 45 min at 37 °C, the digested tissue was minced, forced through a nylon cell strainer of 100 μm (BD Falcon™) and centrifuged. The pellet was resuspended in a gradient of 30% Percoll (Amersham Biosciences) in PBS and centrifuged at 520 g for 30 min at RT to obtain a pellet with brain mononuclear cells.

Spleen and brain mononuclear cells were incubated with anti-mouse Fc block in FACS buffer (2% FCS and 0.01% NaN3 in PBS) for 30 min at 4 °C to block irrelevant binding of the antibodies to the Fc receptor of myeloid cells. After washing, cells were stained

with defined cocktails of fluorochrome-conjugated antibodies (Suppl. Table 3). For intracellular staining, cells were incubated for 5h in RPMI complete medium containing eBioscience™ Cell Stimulation Cocktail (Invitrogen). Cells were then washed and fixed and permeablized with BD Cytofix/Cytoperm™ (BD) before staining with anti-mouse Granzyme B-efluor 450 and anti-mouse IFNγ-PE (BioLegend). Brain cells isolated from *Pba*-infected mice injected with BrdU were stained using the FITC BD BrdU Flow Kit (BD Pharmingen™) according to the manufacturer's instructions. Stained cells were resuspended in FACS buffer with 5,000 of 10-µm counting beads (SureCount™ Standards, Bang Laboratories) and analyzed by flow cytometry (LSR Fortessa X20™, BD). Data were analyzed with FlowJo v10 software and cell types identified according to the gate strategy (Fig. S6)

Isolation of microparticles (MPs) and extracellular particles (EPs)

All the solutions were filtered (0.22 µm) before use. Blood microparticles (MPs) were obtained from mouse blood collected by cardiac puncture with a syringe containing 100 µl of EDTA, 0.5 M. Plasma was prepared by two successive centrifugations at 1500 g for 15 minutes at 4ºC. Harvested plasma was further centrifuged at 20 000g for 25 minutes and the pellet containing MPs was ressuspended in 0.2% BSA in PBS (28).

IE-derived EPs were prepared from the supernatant of IE cultures. Whole blood of *Pba* infected mice (day 5-6 PI, 10-20% parasitaemia) was collected by cardiac puncture with a syringe containing heparin and suspended in 5 ml of RPMI 1640 medium (Biowest), followed by centrifugation at 450*g* for 10 min. The pellet was resuspended in RPMI 1640 medium containing Glutamax and Neomycin (0.05 mg/ml), supplemented with 20% FBS (Biowest) without or with chloroquine, 8 µM, and then incubated in culture flasks overnight in a orbital shaker at 36.5ºC and 50 rpm. EPs were isolated adapting a

previously described procedure (29) (Fig S5A). Briefly, the cell suspension was first centrifuged at 600g to remove IE and non-IE and then centrifuged at 1600g for 15min to remove cell debris. The supernatant of this centrifugation was further sequentially centrifuged at 5630g and 20 000g for 20 min (total EPs). The pellet resulting from centrifugation at 5630g was designated fraction 1 (Fr1) and the supernatant was further centrifuged at 20 000g producing a pellet, "–Fr1". Fr1 was resuspended in PBS and passed through a LS magnetic exclusion column according to the manufacturer's instructions (MACS Milteny Biotec). Particles retained in this column were designated Fr2. The flow through (Fr3) was centrifuged at 10 000g for 10 min and the obtained pellet incubated with biotinylted anti-mouse TER119 antibody (1 μg/ml) (Invitrogen). The pellet was then washed twice and resuspended in 80 μl of labeling buffer (PBS, 2 mM EDTA) containing 20 μl of Anti-Biotin MicroBeads (Milteny Biotec). After incubation for 15 min at 4ºC and washing, the pellet was resuspended in separation buffer (0.5% BSA, 2 mM EDTA in PBS) followed by magnetic separation through a second LS column. Particles retained in this column and flow through were designated Fr4 and Fr5, respectively.

Characterization of EPs

NanoSight

Blood-derived MPs were analyzed for particle concentration and size distribution by the NS300 Nanoparticle Tracking Analysis (NTA) system with a red laser (638 nm) (NanoSight –Malvern Panalytical, United Kingdom). Samples were pre-diluted in PBS to a concentration range of $5x10^7$-$1x10^9$ particles/ml and 10-50 particles/frame for optimal NTA analysis. Video acquisitions were performed using camera level 16 and threshold 5. Five videos of 30s each were captured per sample. Analysis of particle

concentration per milliliter and size distribution were performed using the NTA software v3.4.

Flow cytometry

Blood MPs or IE-derived EPs were pre-incubated with Fc-block and then stained with PE-conjugated anti-mouse Ter119, CD41, CD45 and CD105 antibodies (1:100) (Life Technologies) during 20 min. After staining, the samples were washed in PBS (10 000*g*, 10 min, 4ºC) and the pellet was resuspended in PBS and acquired with flow cytometer LSRFortessa™ (BD Biosciences, run with FACSDiVa software version 6.2) using side scatter of blue violet laser (SSC-BV) and FSC-PMT tuned to detect small particles. PBS was used to set background signal and unstained samples used to define PE-negative particles. Total EPs numbers were calculated using 5000 counting beads (10 µm) in each sample.

Transmission electron microscopy

For negative staining, 5 µl of the pellet of serum MPs in HEPES buffer (10 mM) was adhered to glow discharged Mesh100 grids coated with 2% formvar in chloroform and carbon for 2 min. Following attachment, samples were washed with distilled H_2O and stained with 2% uranyl acetate for 2 min.

EPs samples were fixed with 2% formaldehyde and 2.5% glutaraldehyde in 0.1 M phosphate buffer (PB) overnight at 4ºC. After washing three times, samples were embedded for support in 2% low melting point agarose. After solidifying, samples were post-fixed with 1% osmium tetroxide in 0.1 M PB for 30 min at 4ºC. Samples were then washed in PB and distilled water and pre-stained with 1% tannic acid for 20 min at 4ºC and with 0.5% uranyl acetate for 1h at RT in the dark followed by dehydration using increasing concentrations of ethanol. After dehydration, samples were infiltrated and

embedded using a graded series of Embed-812 epoxy resin polymerized at 60ºC overnight. Ultraphin sections (70 nm) were obtained with a Leica UC7 Ultramicroyome and collected in 2% formvar in chloroform-coated slot grids that were post-stained with 1% uranyl acetate and Reynold's Lead Citrate for 5 min each.

Electron microscopy images were acquired on a FEI Tecnai G2 Spirit BioTWIN transmission electron microscope operating at 120 keV and equipped with an Olympus-SIS Veleta CCD Camera.

Brain endothelial cell cultures

Mouse brains were removed from the skull and kept in a petri dish with HBSS medium (Biowest) on ice. The meninges were removed after transferring the brains to a freezer block covered with gauze and rolling a cotton swab over them. Brain blood vessels were then isolated adapting a previously described procedure (30). Briefly, brains were minced with a blade in 1 ml of HBSS medium and aspirated with a syringe. The tissue was then homogenized pushing it five times through a 23G needle. This homogenate was mixed with equal volume of cold 30% (wt/vol) dextran (MW ~60 kDa) (Sigma) in PBS and centrifuged at 10 000g for 15 min. After centrifugation the myelin top layer was removed and the pellet containing the vessels was suspended in DMEM and passed through a 40-μm cell strainer followed by 5 ml of medium to wash away other cells and myelin debris. The strainer was back-flushed with 5 ml of MCDB 131 to collect the brain vessels. These were digested by adding to the medium 1mg/ml of collagenase type IV (Millipore), 10 μg/ml DNAse (Roche) and 2% FBS, followed by incubation for 2-3 hours at 36.5 ºC in an orbital shaker. The digested vessels were then centrifuged and suspended in EGM™-2 Endothelial Cell Growth Medium-2 BulletKit™ (LONZA) supplemented with GlutaMax (ThermoFisher) and 10% of FBS, and containing 4 μg/ml

puromycin and cultured in 24 well-plates, Medium was changed for fresh medium without puromycin every four days.

When cultures reached 50-80% confluence (~14 days, 95% of the cells are $CD31^+$ by flow cytometry analysis), cells were exposed for 18-20h to different amounts ($2x10^5$-$2x10^6$) of IE and NIE, EPs fractions (Total EPs, -Fr1 and Fr1 to Fr5), MPs (present in 600 µl of serum), or different activators of IFNβ signaling (IFNβ, 1000 U/ml; LPS, 1µg/ml; Poly I:C, 1-5 µg/ml). To inhibit endosome acidification, BECs were pre-incubated for 20 min with 20 mM of NH4Cl before adding the stimuli.

Heme was added as ferric chloride heme (hemin, SIGMA) to BECs at a final concentration range of 10-30 µM. A freshly prepared stock solution was obtained by dissolving hemin in NaOH 0.1 M for 1h at 37ºC and then adding 1M Tris, pH 7.5 to a final concentration of 0.1 M. HCl was added to the solution to bring the pH back to 7.5.

Molecular docking

STING1-c-di-GMP crystal structure (PDB ID: 6S26) was retrieved from Protein Data Bank (PDB). The crystal structure was then prepared using the Molecular Operating Environment (MOE v2019.01) structure preparation wizard by stripping out the water molecules. Hydrogen atoms were added, and protonation states were assigned using Protonate-3D tool at pH=7.4 of the MOE software package. The co-crystallized ligand (c-di-GMP) was also prepared using the MOE software package. The EHT10 force field was used in all minimization steps. Again, hydrogen atoms were added using the Protonate-3D tool at pH=7.4.

C-di-GMP was then removed and re-docked into the corresponding STING1 crystal structure. Self-docking was performed in GOLD v5.7 software using ChemPLP as scoring function. The docking binding site was centered at threonine T263 (Fig. S5G), a

crucial residue for c-di-GMP and STING1 interaction, and a search radius of 15 Å was set. Upon self-docking successfully validated the developed protocol, molecular docking of heme was performed, 500 GA runs. Heme followed the same ligand preparation procedure as c-di-GMP.

Peroxidase activity and gel migration shift assay

Recombinant human STING1 protein (Gentaur) (0.3 μg, 1μM) in 20 mM Tris-HCl, 0.15 M NaCl, pH=8.0 (Tris buffer) was incubated for 15 min at room temperature (RT) with 3000, 600, 300, 150, 60 and 6 μM of heme. After adding Tris sample buffer (pH=6.8) for native PAGE (no SDS or reducing agents), the samples were loaded on 12% Criterion™ TGX™ Stain-Free™ precast gels for PAGE (Bio-Rad). Heme-STING1 complexes were separated by gel electrophoresis in non-denaturing running buffer. Peroxidase-like activity of heme (31) bound to STING1 was detected on the gel after incubation with TMB Substrate Reagent Set (BD Biosciences). After a blue-colored band developing, the gel were washed with 0.5 M sodium acetate (pH=5) and isopropanol (30%). Migration shift of ptotein-heme complexes (32) was examined after washing the gel in Milli-Q water and protein staining for 2 hours at RT with Commassie Brilliant Blue R250 (0.05% in 50% of methanol and 10% of acetic acid in H_2O) followed by incubation with destaining solution (10% etanol and 7.5% acetic acid in H_2O). STING1 without incubation with heme and heme alone were used as negative controls of peroxidase-like activity. Serum bovine albumin (3.3 μg, 5μM) incubated with 600 μM of heme was used as a positive control (33).

Gene expression

RNA was prepared from total mouse brains of mice and from BECs using Trizol and Cells-to-CT kit (Thermo Fisher Scientific), respectively. One microgram of total brain RNA was converted to cDNA (Transcriptor High Fidelity cDNA Synthesis Kit; Roche). A final volume of 20 µl of the cDNA reaction was diluted 1:3 in RNase-free water to be used in qRT-PCR. *Ifnβ1*, *Cxcl10*, *Irf7*, *Irf1* and *Ifit1* mRNA were quantified using Mm00439552_s1, Mm00445235_m1, Mm00516788_m1, Mm01288580_m1 and Mm00515153_m1 TaqMan Gene Expression Assays from ABI, respectively.

IFNβ-luciferase reporter assay

Tissues were lysed in Glo Lysis Buffer (Promega) followed by centrifugation at 20,000g for 20 min. BECs were gently washed with PBS before lysis. 50 µl of tissue or cell lysates were mixed with 50µl of Bright-Glo™ Luciferase Assay System (Promega) in a 96-well luminometer plate. The luminescence was immediately measured with GloMax® Explorer (Promega) (excitation, 405nm; emission, 500-550nm; integration time, 5). Protein was quantified by Bradford Assay (BioRad) and luciferase activity expressed as RFU per mg of protein.

Satistical Analysis

Statistical analysis was performed using Prism v6.01 software (GraphPad Software, Inc.). Comparisons between treated and non-treated conditions used two-tailed unpaired t-test, comparisons between multiple groups used one-way ANOVA, comparisons

between treated cells of different genotypes used two-way ANOVA as indicated in figure legends. Bars in figures represent the mean (±SD) and each symbol represents one mouse or well as indicated in the figures. Sample size and number of independent experiments performed can be found in the figures and figure legends.

Results

IFNβ production in the brain is associated with lethal CM development

There is indirect evidence connecting brain type I IFN responses with tissue pathology associated with CM in *Pba*-infected mice (34,35). We found that this response is wide spread in three main brain regions (i.e, olfactory bulb, cerebrum and cerebellum) as indicated by the expression of four type I IFN response interferon-stimulated genes (*Irf1*, *Irf7*, *Ifit1* and Cxcl10) (Fig. 1A). We used an IFNβ-luciferase reporter mouse line (36) to directly test whether IFNβ induction in the brain was triggered by *Pba* infection. We detected strong luminescence (Fig. S1A) and significantly increased luciferase activity in brain tissue as well as in the lung of mice developing CM (Fig. 1B). On the other hand, mice infected with *PbNK65,* a parasite strain that does not cause CM, induced weak or no luminescence signal (Fig. S1B). This suggested that IFNβ production and the ensuing type I IFN response in the brain was associated with CM development.

BBB leakage was significantly decreased in IFNβ KO mice as shown by decreased brain staining in mice perfused with EB at day 6 PI (Fig. 1C and 1SC). Accordingly, IFNβ KO mice showed lower lethality of CM than WT controls (Fig 1D). Decreased lethality due to CM in IFNβ KO mice was not attributable to differences in parasite burden and was not affected by sex (Fig. 1SD). These data indicated that type I IFN responses within the brain that are mounted in the context of CM contribute to BBB disruption and brain tissue damage, which culminate in death.

STING1 contributes to CM lethality and promotes IFNβ production

We next searched for mediators of type I IFN response induction involved in CM lethality. It has been shown that during *Plasmodium* infection, specific PRRs, namely TLRs, sense plasmodial GPI anchors and unmethylated CpG motifs of plasmodial DNA signal through MyD88 or TRIF (reviewed in (37)). Also, RIG-I-like receptors (RLRs), such as melanoma differentiation-associated gene 5 (MDA5) respond to *Plasmodium* RNA engaging MAVS in the mitochondria (37). In addition, the cGAS-STING1 pathway of type I IFN induction has been recently shown to be activated in monocytes by parasite DNA contained in internalized EPs that are released from *P. falciparum*-IE (20). Downstream signaling of these receptors converge at the phosphorylation and activation of type I Interferon regulatory family of transcription factors (IRFs) (38).

We analyzed infection survival curves of MyD88 KO and TRIF KO mice that are deficient in TLR and IL-1R signaling, (Fig. 2A), and MDA5 KO, MAVS KO and STING1 KO mice with deficiencies in RNA and DNA sensing (Fig. 2B). We found that only *Sting1* deletion significantly delayed death by CM and conferred approximately 50% protection against CM lethality. Although we cannot exclude minor contributions of the other receptors, we did not detect a significant difference in CM lethality when STING1 KO mice were compared with quadruple KO mice for *Myd88*, *Trif*, *Mavs* and *Sting1* (MyTrMaSt KO) that are impaired in all known type I response induction pathways (Fig. S1E). CM protection in STING1 KO mice was associated with lower levels of IFNβ induction as noted in the brain of IFNβ-reporter mice deficient for STING1 (Fig. 2C). These results indicate that STING1 is a major innate immune sensor of *Pba* infection mediating IFNβ production in the brain and subsequent CM development.

STING1 activation induces *Cxcl10* gene expression and leukocyte recruitment to the brain

It has been previously shown that innate immune responses occur in the brain before leukocyte infiltration in *Pba*-infected mice (27,39). Using IFNβ-reporter mice in both alleles, we detected a significant increase of luciferase activity in the brain of mice as early as day 4 post-infection, due to *Ifnβ1* gene promoter activation (Fig. 3A). Therefore, we investigated whether IFNβ induction by STING1 in the brain was driving expression of *Cxcl10* in the brain, a known mediator of leukocyte recruitment, previously detected in brain endothelial cells in CXCL10-reporter mice at day 4 post-infection (40). Deletion of *Ifnβ1* or *Sting1* significantly decreased the levels of *Cxcl10* mRNA in the brain, at day 4 post-infection (Fig. 3B).

Several reports indicate that *Plasmodium* infection induces CXCL10 in the brain, which recruits CXCR3 expressing antigen-specific $CD8^+$ T cells that interact with the brain endothelium leading to CM (40–42). Therefore, we investigated whether brain leukocyte infiltration was affected in IFNβ KO and STING1 KO mice. We found lower percentage (Fig. 3C) and numbers of leukocytes ($CD45^{high}$), namely $CD8^+$ T cells ($CD45^+TCR\beta^+CD8^+$) and monocytes ($CD45^{high}$ $Mac1^+$), in brain of STING1 KO mice (Fig. 3D) and IFNβ KO mice (Fig. S3A). However, based on similar expression of $CD8^+$ T cell surface activation markers ($CD44^{high}$/ $CD62L^{low}$) and of Granzyme B and IFNγ, $CD8^+$ T cell activation was comparably effective in wild type, STING1 KO (Fig. 3D) and IFNβ KO mice (Fig.S3A). In addition, the low numbers of $CD8^+$ T cells in the brain of infected of STING1 KO mice could not be attributed to decreased local

proliferation (27) as the frequency of $BrdU^+$ cells amongst $CD8^+$ T cells was 44.5% ± 7.74 compared to 33.7% ± in 6.95 in wild type mice. Furthermore, microglia activation assessed by MHC class I (27) expression was similar in wild type and KO mice (Fig. 3D and S3A).

Importantly, a decrease in the number of brain-infiltrating leukocytes in the brain was not related to a decrease in the activation of splenic T cells or monocytes in STING1 KO or IFNβ KO mice (Fig. S3B). This suggests that innate immune activation of STING1 leading to IFNβ production and *Cxcl10* gene up-regulation in the brain contributes to the recruitment of leukocytes into the brain during CM development. We hypothesized that STING1-dependent induction of IFNβ in the brain cells contributes to brain immunopathology in CM**.**

STING1 activation and IFNβ production by brain endothelial cells contributes to CM pathology

Although induction of type I IFN via TLR-dependent and independent receptors has been reported in glial and neuronal cells during brain viral infection (43), it is unclear whether specific brain cell types are responsible for the induction of IFNβ response to blood-borne parasites. IFNβ production in different brain cell types during CM was investigated in cell type-specific IFNβ-reporter mice generated by breeding $IFN\beta^{flox\beta\text{-}luc/flox\beta\text{-}luc}$ animals with mice that drive cell-type specific Cre expression (44). In these mice one *Ifnβ1* allele is kept wild-type while the other allele drives luciferase activity by the *Ifnβ1* floxed allele in cells that undergo Cre recombination. We found no significant induction of luciferase activity in $GFAPCre^+$ (astrocytes) mice with CM while a clear response was obtained to Poly I:C injection (Fig. 4A). On the other hand, $LysMCre^+$

brain cells, that in CM context may include microglia cells and blood-recruited inflammatory monocytes (27), showed *Ifnβ1* transcription activation in infected mice as detected by increased luciferase activity in the brain (Fig. 4B).

To determine whether IFNβ is induced in microglia during CM, we targeted this tissue resident macrophage population in CR3CX1CreERT2$^{+/-}$ mice (45). After Cre induction with tamoxifen, we awaited replenishment of the monocyte compartment with bone-marrow derived cells without flox excision while self-renewing microglia maintains the *Ifnβ1*-luc reporter gene active. Under these conditions, we found significant increase in luciferase activity indicating that the *Ifnβ1* gene promoter was activated in the microglial cell compartment during CM (Fig. 4C).

Induction of *Ifnβ1* in the endothelial compartment was assessed in reporter mice that express Cre in endothelial and hematopietic cells under the Tie2 promoter (Fig. 4D), and in reporter mice carrying inducible Cre under the Slco1c1 promoter activated specifically in brain endothelial/ependymal cells (46) (Fig. 4E). Induction of luciferase activity in both mouse lines implied that brain endothelial cells contribute to local brain production of IFNβ in the brain during CM.

To determine whether expression of STING1 or IFNβ in specific cell types cells impact CM development, we used mice with cell-lineage specific Cre expression and carrying two floxed alleles or one inactivated allele and one floxed allele for the target gene. We found that absence of STING1 or IFNβ in LysM^{+} or CX3CR1^{+} cells did not prevent mice from dying of CM (Fig. 4F and S3A). However, ablation of STING1 or IFNβ in endothelial and hematopoietic cells in mice expressing Cre under Tie2 promoter (Fig. 4G and S3B) or ablation of STING1 specifically in brain endothelial cells in Slco1c1CreERT mice significantly protected from CM lethality (Fig. 4H) and improved

health/neurologic score from day 6 (Fig S3C) without affecting parasitemia (Fig. S3D). Conditional STING1 KO mice in the Tie2^{+} cell compartment that did not die with CM, showed clinical improvement over time (Fig. S3E), while parasite burden was not reduced (Fig. S3F).

Overall, these results unveil that STING1-dependent activation of IFNβ production in brain endothelial cells starting early in infection is a critical determinant of brain immunopathology during CM development.

Induction of IFNβ in brain endothelial cells by IE-derived EPs requires STING1 and intracellular acidification

The generation of extracellular microparticles (MPs; 100-1000 nm) by erythrocytes has been associated with the pathogenesis of human and rodent CM (47,48). Also, vesicles released from *P. falciparum*-IE activate expression of pro-inflammatory cytokines (i.e TNF and IFNβ) in innate immune cells (20,29). We asked whether MPs and *P. berghei*-IE derived particles can induce type I IFN signaling in primary brain endothelial cells (BECs) cultures.

Nanoparticle tracking analysis of MPs collected from the serum of *Pba*-infected and seek mice show a significant increase in mean size compared to non-infected mice (Fig. 5A). Accordingly, negative-stain transmission electron microscopy (TEM) (Fig. 5B) and size profile of particles obtained from infected animals (Fig. S4A) show particles larger than 200 nm while those isolated from non-infected animals are within the size range of exosomes (around 100 nm) (Fig. 5A and 5B). Moreover, the concentration of particles within the range of 100.5-265.5 nm increased approximately 3 fold in the blood of infected mice with CM in comparison to non-infected controls (Fig. S4B). The

particles isolated from blood of *Pba*-infected mice that differ from non-infected mice were mostly from leukocyte ($CD45^+$) and erythrocytic origin ($TER119^+$) as revealed by antibody staining of cell-type specific surface markers (Fig. 5C).

In BECs cultures, particles isolated from blood of mice with CM but not from non-infected animals activate IFNβ gene transcription (Fig 5D) and protein expression (Fig. S4B). Similarly, extracellular particles (EPs) obtained by high-speed centrifugation from IE cultures activate *Ifnβ1* transcription measured by the luciferase activity in IFNβ-reporter BECs (Fig. 5E). On the other hand, neither erythrocytes from non-infected mice (NIE) nor from *Pba*-infected mice (IE) induce luciferase activity (Fig. 5E). To determine whether endosomal acidification was required for endothelial response, cells were pretreated cells with ammonium chloride, which elevates the intralysosomal pH (49). Remarkably, induction of IFNβ in response to EPs was abolished in BECs pre-exposed to ammonium chloride (Fig. 5F). In addition, *Sting1* deletion reduced luciferase activity in IFNβ-reporter BECs incubated with IE-derived EPs (Fig. 5G). These data indicate that particles produced by infected erythrocytes that are up taken up and processed in acidic compartments in BECs activate STING1 leading to induction of IFNβ.

Parasite-sequestered heme induces *Ifnβ1* and *Cxcl10* in brain endothelial cells

To identify bioactive factors associated with EPs that trigger type I IFN response in brain endothelial cells, we established a protocol to fractionate bulk EPs obtained from *P. berghei*-IE cultures on basis of a combination of differential centrifugation, paramagnetic separation and presence of host erythrocytic membrane (Fig. S5A). We found that the fraction (Fr1) pulled down at lower centrifugation (5630 g) induced even

stronger *Ifnβ1* transcription measured by luciferase activity compared to the total EPs (Fig. S5B). Therefore, we further fractionated Fr1 using a magnetic LS column to separate a fraction enriched in particles containing iron and hemozoin (Fr2) from the flow through (Fr3) (Fig. S5A). To isolate particles with erythrocytic membrane, Fr3 was incubated with biotinylated anti-TER119 antibody and streptavidin magnetic beads (Fig. S5A). The retained fraction in immuno-magnetic separation and the flow through originated Fr4 and Fr5, respectively. Flow cytometry analysis (Fig. 6A and Fig. S5D) showed that Fr2 and Fr5 are enriched in TER119^{-} particles indicating a low content in particles with erythrocytic membrane (TER119^{+}) in comparison with the initial Fr1. Fr5 contained parasite-derived material as denoted by GFP signal, originated from the *Pba*-GFP parasite used in the IE cultures. TEM of fixed samples confirmed that Fr2 contained vesicles with hemozoin crystals likely deriving from digestive vacuoles (Fig. 6B). Among all fractions, the hemozoin-enriched Fr2, strongly induced luciferase activity in BECs at a 10-fold lower amount ($2x10^5$ EPs) (Fig. 6C) compared to total EPs ($2x10^6$ EPs). In these assays, Fr2 was also a potent inducer of *Cxcl10* (Fig. 6D) and *Irf7* (Fig. S5E) two downstream effectors of IFN stimulation response. However, expression of these genes was about two-fold lower in STING KO BECs and was abolished in IFNβ KO and in quadruple MyTrMaSt KO BECs (Fig. 6D and Fig. S5E). The same amount of IE, Fr1 or in Fr-1 particles (the remaining particles in the supernatant pull down at 20 000 g after removing Fr1) did not significantly induced *Cxcl10* and *Irf7* gene expression (Fig. 6D and Fig. S5E). As *Cxcl10* and *Irf7* induction by IFNβ-IFNAR pathway was preserved in BECS from those KO models (Fig. S5F).

We then addressed the role of hemozoin in STING1 activation by inhibiting the hemozoin synthesis pathway in IE cultures with chloroquine, also described to increase levels of labile heme in the parasite (50). Unexpectedly, we found that IFNβ induction

was stronger using EPs obtained from chloroquine-treated cultures (Fig. 6E). Both hemozoin and labile heme can activate PRRs contributing to the inflammatory storm and BBB dysfunction in CM (17,18,51). Thus, we directly stimulated BECs with different amounts of heme and hemozoin. While hemozoin was unable to stimulate BECs, heme at 20 uM, significantly induced luciferase activity in wild-type but not in STING1 KO IFNβ-reporter cells (Fig. 6F and S5G). Moreover, heme induced *Cxcl10* gene expression in brain endothelial cells, as previously described (52,53), which was not observed in STING1 KO BECs (Fig. 6G).

To inquire about a putative interaction of heme with STING1 we performed docking calculations. Heme was docked into the structure of STING1 using GOLD software and searching for the optimal pose (orientation, conformation and binding energy) between heme and STING1. We found that the heme is positioned in exactly the same region, within the STING1 binding site, and is mostly overlapped with the c-di-GMP (Fig. 6H), showing that the molecule can position itself in a propitious way in the pocket and will be able to interact with the STING1. Although well positioned, heme has less affinity to STING1 with a ChemPLP score of 61 compared to 104 for c-di-GMP.

We tested the ability of STING1 to bind heme by examining the peroxidase-like activity and migration shift of recombinant human STING1 incubated with heme. We detected peroxidase activity of STING1-heme complexes at the molar ratio of 1:150 while protein shift was detected at a molar ratio of 1:60 (Fig 6I), similar to what has been reported by other heme-binding proteins in this assay (32).

Taken together, the results indicate that heme-containing EPs derived from IE are able to induce type I IFN responses in BECs in a STING1-dependent manner, possiblye involving direct heme binding to STING1.

Discussion

We identified STING1 activation in brain endothelial cells as a molecular pathway that mediates neuroinflammation and brain pathology associated with the pathogenesis of CM. We demonstrated that, early in infection, brain endothelium uses STING1 to sense *Plasmodium* blood-stage infection and initiate a type I IFN response by activating *Ifnβ1* and *Cxcl10* gene transcription. This is associated with leukocyte recruitment and subsequent loss of BBB function, a hallmark of CM. We found that IE-derived extracellular particles enriched for hemozoin-containing vesicles and for labile heme trigger STING1-dependent IFNβ responses in brain endothelial cells.

Our study identifies IFNβ as a critical type I IFN molecule that triggers IFNAR signaling, and determines BBB disruption and lethality in CM. Whole and cell-specific IFNβ-reporter mice enabled us to identify STING1 as the key PRR upstream of IFNβ production by brain monocytes/microglia and brain endothelial cells. Being a main activator of *Ifnβ1*transcription, STING1 also controlled early *Cxcl10* gene induction in the brain of *Pba*-infected mice. CXCL10 is known to promote chemotaxis of CXCR3 expressing $CD8^+$ T cells to the central nervous system during *Toxoplasma* infection (42) and has been strongly linked to CM severity both in humans and in rodents. The CXCL10 levels detected in post-mortem samples of blood and cerebral spinal fluid were higher in fatal cases of CM than in non-cerebral fatal cases or non-complicated malaria cases (54,55). In mice, deletion of *Cxcl10* gene partially protected from CM lethality (41). Our data support a role for CXCL10 in inducing chemotactic leukocyte migration into the brain. We observed that both IFNβ KO and STING1 KO have lower numbers of $CD8^+$ T cells and monocytes in the brain infiltrates. In agreement, *in vivo* imaging studies showed that endothelial CXCL10 strengthened the interactions of brain endothelium with pathogenic $CD8^+$ T cells during CM (40). Moreover, CXCL10 may

also act on neurons. IFNAR-dependent induction of CXCL10 in brain endothelium was shown to promote virus-induced sickness behavior, namely by binding to CXCR3 on neurons and changing synaptic plasticity (47). A similar mechanism may operate during CM and contribute to the neurologic symptoms and cognitive impairments in survivors.

We provide the first demonstration that activation of STING1 in BECs promotes CM pathology. Infected mice whose brain endothelial/ependymal cells are made deficient in STING1 (Slco1c1CreERT STING1 floxed mice) displayed milder neurological deficits and increased survival. Several studies reported that plasmodial DNA activates STING1 in innate immune cells such as monocytes and macrophages (20–22). However, we found that specific *Ifnβ1* or *Sting1* deletion in myeloid and microglia cells did not affect CM development in mice. Still, *Sting1* deletion in mice or BECs did not completely abolish *Pba*-induced expression of *Ifnβ1* or *Cxcl10*. This was only achieved when several PRRs (MyD88, TRIF, MAVS and STING1) were absent in BEC cells. It is possible that STING1 also operates in CM through IFN-independent pathogenic cellular pathways such as autophagy (56) or T cell apoptosis induced by calcium signaling activation and endoplasmatic reticulum (ER) stress (57).

STING1 is localized in the ER and does not bind DNA directly, but interacts with cyclic dinucleotides, namely cGAMP. cGAMP is produced by cyclic-GMP-AMP synthase (cGAS) upon dsDNA sensing in the cytosol. After translocation into the Golgi apparatus, STING1 and TBK1 phosphorylate IRF3 that promotes transcription of type I IFN genes (58). Synthesized Plasmodial DNA, in particular falciparum AT-rich stem-loop DNA motifs, were shown to induce STING1-dependent transcription of IFNβ in macrophages (22). Interestingly, a population of exosomes isolated from *P. falciparum* (Pf) IE cultures at the ring stage, could transfer Pf-DNA to PBMCs and activate cGAS-STING1 release into cytosol with consequent induction of *Ifn*β1/α gene expression

(20). This highlights the likely important role for IE-derived particles in the activation of innate immune mechanisms during malarial infection. Nanoparticle tracking and transmission electron microscopy improved the characterization of blood MPs in mice with CM. We showed increased amounts of MPs, mainly of erythrocytic origin, in the blood thereby confirming previous flow cytometry studies (48,59). Furthermore, we found that IE-derived particles larger than exosomes and enriched in vesicles containing hemozoin are able to activate *Ifnβ* and *Cxcl10* transcription in BECs. This activation depends on intracellular organelle acidification suggesting a requirement for endosome maturation and/or acidic hydrolase activity (49). IE-derived particles containing hemozoin could represent digestive vacuoles that accumulate heme and/or hemoglobin. Although plasmodial DNA-bound to hemozoin has been shown to activate cyclic GMP-AMP (cGAS) upstream STING1 in macrophages (13), hemozoin itself does not seem to be required for STING1 activation in BECs. In fact, exposure of IE to chloroquine, which reduces hemozoin and increases labile heme bioavailability, enhances IFNβ in BECs. This prompted us to hypothesize that heme could be involved in STING1 activation mediated by IE-derived EPs. Indeed, we observed STING1-dependent up-regulation of *Ifnβ* and *Cxcl10* in the presence of labile heme at concentrations within the ranges found in the plasma of children with CM (60) and known to activate *Cxcl10* transcription in endothelial cells (52). Previous studies have shown that heme activates macrophages and endothelial cells through a TLR4-dependent mechanism (52,61). Together, these data reinforce the notion that heme released by hemolysis, namely in malaria infection, can act as an alarmin and modulate both innate and adaptive immune responses (17). Recently, hemolysis in sickle cell disease and injection of hemin in mice were shown to activate and recruit monocytes to the liver through activation of type I IFN signaling and independently of TLR4. (62). Further evidence of direct binding of

heme to STING1 in the ER is required to clarify whether heme is a direct or indirect activator of STING1 in BECs. Interestingly, late endosomes tightly contact with the ER (63) indicating that heme-STING1 interaction may occur during the association between acidified mature endosomes containing heme and the ER.

Overall, we demonstrate that STING1 in the brain endothelium senses molecular by-procucts of erythrocyte infection by *Plasmodium* infection, such as labile heme, initaiting to a type I IFN response mediated by IFNβ with induction of CXCL10 in early phases of infection. This, in turn, triggers a cascade of events that promote brain inflammation, including leukocyte recruitment, and may also affect neuronal responses. This study suggests that type I IFN targeted strategies may minimize brain immunopathology, thus preventing fatal CM and subsequent neurological sequels in survivors.

Acknowledgments

This work was supported by ERA-NET NEURON.

We gratefully acknowledge the Electron Microscopy Unit at IGC, in particular Ana Laura Sousa for technical support. We thank M. Soares and S. Gomes for discussions and critical reading of the manuscript.

Author contributions

Conceptualization, T.F.P. and C.P.G.; investigation, T.F.P., H.A., J.M.S., N.D., R.N., M.C.S.M., B.C.S., R.C.A., R.C.G. and C.C., methodology, T.F.P., H.A., M.C.S.M, R.C.A., R.C.G. and C.C.; project administration, T.F.P and C.P.G, formal analysis, T.F.P., H.A., J.M.S.; resources, M.C.S.M., B.C.S., C.C., U.K.; writing, T.F.P., C.P.G., N.D.; funding acquisition, C.P.G.; supervision, T.F.P., C.P., R.C.G., U.K.

References

1. Idro R, Marsh K, John CC, Newton CRJ. Cerebral malaria: Mechanisms of brain injury and strategies for improved neurocognitive outcome. *Pediatr Res* (2010) **68**:267–274. doi:10.1203/PDR.0b013e3181eee738

2. Mohanty S, Benjamin LA, Majhi M, Panda P, Kampondeni S, Sahu PK, Mohanty A, Mahanta KC, Pattnaik R, Mohanty RR, et al. Magnetic Resonance Imaging of Cerebral Malaria Patients Reveals Distinct Pathogenetic Processes in Different Parts of the Brain. *mSphere* (2017) **2**:e00193–17. doi:10.1128/mSphere.00193-17

3. Seydel KB, Kampondeni SD, Valim C, Potchen MJ, Milner D a., Muwalo FW, Birbeck GL, Bradley WG, Fox LL, Glover SJ, et al. Brain Swelling and Death in Children with Cerebral Malaria. *N Engl J Med* (2015) **372**:1126–1137. doi:10.1056/NEJMoa1400116

4. Dunst J, Kamena F, Matuschewski K. Cytokines and Chemokines in Cerebral Malaria Pathogenesis. *Front Cell Infect Microbiol* (2017) **7**: doi:10.3389/fcimb.2017.00324

5. Frevert U, Nacer A. Fatal cerebral malaria: a venous efflux problem. *Front Cell Infect Microbiol* (2014) **4**:1–7. doi:10.3389/fcimb.2014.00155

6. Sebina I, Haque A. Effects of type I interferons in malaria. *Immunology* (2018) **155**:176–185. doi:10.1111/imm.12971

7. Boldt ABW, van Tong H, Grobusch MP, Kalmbach Y, Dzeing Ella A, Kombila M, Meyer CG, Kun JFJ, Kremsner PG, Velavan TP. The blood transcriptome of childhood malaria. *EBioMedicine* (2019) **40**:614–625. doi:10.1016/j.ebiom.2018.12.055

8. Krupka M, Seydel K, Feintuch CM, Yee K, Kim R, Lin CY, Calder RB, Petersen C, Taylor T, Daily J. Mild Plasmodium falciparum malaria following an episode of severe malaria is associated with induction of the interferon pathway in Malawian children. *Infect Immun* (2012) **80**:1150–1155. doi:10.1128/IAI.06008-11

9. Vigário AM, Belnoue E, Grüner AC, Mauduit M, Kayibanda M, Deschemin J-C, Marussig M, Snounou G, Mazier D, Gresser I, et al. Recombinant Human IFN-α Inhibits Cerebral Malaria and Reduces Parasite Burden in Mice. *J Immunol* (2007) **178**:6416–6425. doi:10.4049/jimmunol.178.10.6416

10. Hassan A, Wlodarczyk MF, Benamar M, Bassot E, Salvioni A, Kassem S, Berry A, Saoudi A, Blanchard N. A virus hosted in malaria-infected blood protects against T cell-mediated inflammatory diseases by impairing DC function in a type I IFN-dependent manner. *MBio* (2020) **11**: doi:10.1128/mBio.03394-19

11. Ball EA, Sambo MR, Martins M, Trovoada MJ, Benchimol C, Costa J, Antunes Gonçalves L, Coutinho A, Penha-Gonçalves C. IFNAR1 controls progression to cerebral malaria in children and CD8+ T cell brain pathology in Plasmodium berghei-infected mice. *J Immunol* (2013) **190**:5118–27. doi:10.4049/jimmunol.1300114

12. Edwards CL, Best SE, Gun SY, Claser C, James KR, de Oca MM, Sebina I, Rivera FDL, Amante FH, Hertzog PJ, et al. Spatiotemporal requirements for IRF7 in mediating type I IFN-dependent susceptibility to blood-stage Plasmodium infection. *Eur J Immunol* (2015) **45**:130–141. doi:10.1002/eji.201444824

13. Sharma S, DeOliveira RB, Kalantari P, Parroche P, Goutagny N, Jiang Z, Chan J, Bartholomeu DC, Lauw F, Hall JP, et al. Innate Immune Recognition of an AT-Rich Stem-Loop DNA Motif in the Plasmodium falciparum Genome. *Immunity* (2011) **35**:194–207. doi:10.1016/j.immuni.2011.05.016

14. Torre S, Polyak MJ, Langlais D, Fodil N, Kennedy JM, Radovanovic I, Berghout J, Leiva-Torres GA, Krawczyk CM, Ilangumaran S, et al. USP15 regulates type i interferon response and is required for pathogenesis of neuroinflammation. *Nat Immunol* (2017) **18**:54–63. doi:10.1038/ni.3581

15. Gazzinelli RT, Kalantari P, Fitzgerald KA, Golenbock DT. Innate sensing of malaria parasites. *Nat Rev Immunol* (2014) **14**:744–757. doi:10.1038/nri3742

16. Francis SE, Sullivan DJ, Goldberg DE. Hemoglobin metabolism in the malaria parasite Plasmodium falciparium. *Annu Rev Microbiol* (1997) **51**:97–123. doi:10.1146/annurev.micro.51.1.97

17. Soares MP, Bozza MT. Red alert: Labile heme is an alarmin. *Curr Opin Immunol* (2016) **38**:94–100. doi:10.1016/j.coi.2015.11.006

18. Pamplona A, Ferreira A, Balla J, Jeney V, Balla G, Epiphanio S, Chora Â, Rodrigues CD, Gregoire IP, Cunha-Rodrigues M, et al. Heme oxygenase-1 and carbon monoxide suppress the pathogenesis of experimental cerebral malaria. *Nat Med* (2007) **13**:703–710. doi:10.1038/nm1586

19. Ferreira A, Marguti I, Bechmann I, Jeney V, Chora Â, Palha NR, Rebelo S, Henri A, Beuzard Y, Soares MP. Sickle hemoglobin confers tolerance to plasmodium infection. *Cell* (2011) **145**:398–409. doi:10.1016/j.cell.2011.03.049

20. Sisquella X, Ofir-Birin Y, Pimentel MA, Cheng L, Abou Karam P, Sampaio NG, Penington JS, Connolly D, Giladi T, Scicluna BJ, et al. Malaria parasite DNA-harbouring vesicles activate cytosolic immune sensors. *Nat Commun* (2017) **8**: doi:10.1038/s41467-017-02083-1

21. Gallego-Marin C, Schrum JE, Andrade WA, Shaffer SA, Giraldo LF, Lasso AM, Kurt-Jones EA, Fitzgerald KA, Golenbock DT. Cyclic GMP–AMP Synthase Is the Cytosolic Sensor of Plasmodium falciparum Genomic DNA and Activates

Type I IFN in Malaria . *J Immunol* (2018) **200**:768–774. doi:10.4049/jimmunol.1701048

22. Sharma S, DeOliveira RB, Kalantari P, Parroche P, Goutagny N, Jiang Z, Chan J, Bartholomeu DC, Lauw F, Hall JP, et al. Innate Immune Recognition of an AT-Rich Stem-Loop DNA Motif in the Plasmodium falciparum Genome. *Immunity* (2011) **35**:194–207. doi:10.1016/j.immuni.2011.05.016

23. Howland SW, Poh CM, Rénia L. Activated Brain Endothelial Cells Cross-Present Malaria Antigen. *PLOS Pathog* (2015) **11**:e1004963. doi:10.1371/journal.ppat.1004963

24. Jambou R, Combes V, Jambou MJ, Weksler BB, Couraud PO, Grau GE. Plasmodium falciparum adhesion on human brain microvascular endothelial cells involves transmigration-like cup formation and induces opening of intercellular junctions. *PLoS Pathog* (2010) **6**:1–13. doi:10.1371/journal.ppat.1001021

25. Franke-Fayard B, Trueman H, Ramesar J, Mendoza J, Van Der Keur M, Van Der Linden R, Sinden RE, Waters AP, Janse CJ. A Plasmodium berghei reference line that constitutively expresses GFP at a high level throughout the complete life cycle. *Mol Biochem Parasitol* (2004) **137**:23–33. doi:10.1016/j.molbiopara.2004.04.007

26. Carroll RW, Wainwright MS, Kim KY, Kidambi T, Gómez ND, Taylor T, Haldar K. A rapid murine coma and behavior scale for quantitative assessment of murine cerebral malaria. *PLoS One* (2010) **5**:1–12. doi:10.1371/journal.pone.0013124

27. Pais TF, Chatterjee S. Brain macrophage activation in murine cerebral malaria precedes accumulation of leukocytes and CD8+ T cell proliferation. *J Neuroimmunol* (2005) **163**:73–83. doi:10.1016/j.jneuroim.2005.02.009

28. Dinkla S, Brock R, Joosten I, Bosman GJ. Gateway to understanding microparticles: Standardized isolation and identification of plasma membrane-derived vesicles. *Nanomedicine* (2013) **8**:1657–1668. doi:10.2217/nnm.13.149

29. Mantel PY, Hoang AN, Goldowitz I, Potashnikova D, Hamza B, Vorobjev I, Ghiran I, Toner M, Irimia D, Ivanov AR, et al. Malaria-infected erythrocyte-derived microvesicles mediate cellular communication within the parasite population and with the host immune system. *Cell Host Microbe* (2013) **13**:521–534. doi:10.1016/j.chom.2013.04.009

30. Howland SW, Gun SY, Claser C, Poh CM, Rénia L. Measuring antigen presentation in mouse brain endothelial cells ex vivo and in vitro. *Nat Protoc* (2015) **10**:2016–2026. doi:10.1038/nprot.2015.129

31. Hopp MT, Schmalohr BF, Kühl T, Detzel MS, Wißbrock A, Imhof D. Heme Determination and Quantification Methods and Their Suitability for Practical Applications and Everyday Use. *Anal Chem* (2020) **92**:9429–9440. doi:10.1021/acs.analchem.0c00415

32. Karnaukhova E, Rutardottir S, Rajabi M, Wester RosenlÃ¶f L, Alayash AI, Ã…kerstrÃ¶m B. Characterization of heme binding to recombinant Î±1-microglobulin. *Front Physiol* (2014) **5**:465. doi:10.3389/fphys.2014.00465

33. Englert FA, Seidel RA, Galler K, Gouveia Z, Soares MP, Neugebauer U, Clemens MG, Sponholz C, Heinemann SH, Pohnert G, et al. Labile heme impairs hepatic microcirculation and promotes hepatic injury. *Arch Biochem Biophys* (2019) **672**:108075. doi:10.1016/j.abb.2019.108075

34. Lovegrove FE, Gharib SA, Patel SN, Hawkes CA, Kain KC, Liles WC. Expression microarray analysis implicates apoptosis and interferon-responsive mechanisms in susceptibility to experimental cerebral malaria. *Am J Pathol* (2007) **171**:1894–1903. doi:10.2353/ajpath.2007.070630

35. Berghout J, Langlais D, Radovanovic I, Tam M, MacMicking JD, Stevenson MM, Gros P. Irf8-Regulated Genomic Responses Drive Pathological Inflammation during Cerebral Malaria. *PLoS Pathog* (2013) **9**: doi:10.1371/journal.ppat.1003491

36. Lienenklaus S, Cornitescu M, Ziętara N, Łyszkiewicz M, Gekara N, Jabłońska J, Edenhofer F, Rajewsky K, Bruder D, Hafner M, et al. Novel Reporter Mouse Reveals Constitutive and Inflammatory Expression of IFN-β In Vivo. *J Immunol* (2009) **183**:3229–3236. doi:10.4049/jimmunol.0804277

37. Gowda DC, Wu X. Parasite Recognition and Signaling Mechanisms in Innate Immune Responses to Malaria. *Front Immunol* (2018) **9**:3006. doi:10.3389/fimmu.2018.03006

38. Wu J, Chen ZJ. Innate Immune Sensing and Signaling of Cytosolic Nucleic Acids. *Annu Rev Immunol* (2014) **32**:461–488. doi:10.1146/annurev-immunol-032713-120156

39. Torre S, Polyak MJ, Langlais D, Fodil N, Kennedy JM, Radovanovic I, Berghout J, Leiva-Torres GA, Krawczyk CM, Ilangumaran S, et al. USP15 regulates type i interferon response and is required for pathogenesis of neuroinflammation. *Nat Immunol* (2017) **18**:54–63. doi:10.1038/ni.3581

40. Sorensen EW, Lian J, Ozga AJ, Miyabe Y, Ji SW, Bromley SK, Mempel TR, Luster AD. CXCL10 stabilizes T cell-brain endothelial cell adhesion leading to the induction of cerebral malaria. *JCI insight* (2018) **3**: doi:10.1172/jci.insight.98911

41. Campanella GS V, Tager AM, El Khoury JK, Thomas SY, Abrazinski TA, Manice LA, Colvin RA, Luster AD. Chemokine receptor CXCR3 and its ligands CXCL9 and CXCL10 are required for the development of murine cerebral malaria. *Proc Natl Acad Sci U S A* (2008) **105**:4814–9. doi:10.1073/pnas.0801544105

42. Harris TH, Banigan EJ, Christian DA, Konradt C, Wojno EDT, Norose K, Wilson EH, John B, Weninger W, Luster AD, et al. Generalized Lévy walks and

the role of chemokines in migration of effector CD8 + T cells. *Nature* (2012) **486**:545–548. doi:10.1038/nature11098

43. Owens T, Khorooshi R, Wlodarczyk A, Asgari N. Interferons in the central nervous system: A few instruments play many tunes. *Glia* (2014) **62**:339–355. doi:10.1002/glia.22608

44. Solodova E, Jablonska J, Weiss S, Lienenklaus S. Production of IFN-β during listeria monocytogenes infection is restricted to monocyte/macrophage lineage. *PLoS One* (2011) **6**:2–11. doi:10.1371/journal.pone.0018543

45. Yona S, Kim KW, Wolf Y, Mildner A, Varol D, Breker M, Strauss-Ayali D, Viukov S, Guilliams M, Misharin A, et al. Fate Mapping Reveals Origins and Dynamics of Monocytes and Tissue Macrophages under Homeostasis. *Immunity* (2013) **38**:79–91. doi:10.1016/j.immuni.2012.12.001

46. Ridder DA, Lang MF, Salinin S, Röderer JP, Struss M, Christiane MG, Schwaninger M. TAK1 in brain endothelial cells mediates fever and lethargy. *J Exp Med* (2011) **208**:2615–2623. doi:10.1084/jem.20110398

47. Pankoui Mfonkeu JB, Gouado I, Fotso Kuaté H, Zambou O, Amvam Zollo PH, Grau GER, Combes V. Elevated Cell-Specific Microparticles Are a Biological Marker for Cerebral Dysfunctions in Human Severe Malaria. *PLoS One* (2010) **5**:13415. doi:10.1371/journal.pone.0013415

48. El-Assaad F, Wheway J, Hunt NH, Grau GER, Combes V. Production, Fate and Pathogenicity of Plasma Microparticles in Murine Cerebral Malaria. *PLoS Pathog* (2014) **10**: doi:10.1371/journal.ppat.1003839

49. Mellman I, Fuchs R, Helenius A. ACIDIFICATION OF THE ENDOCYTIC AND EXOCYTIC PATHWAYS. *Annu Rev Biochem* (1986) **55**:663–700. doi:10.1146/annurev.bi.55.070186.003311

50. Fong KY, Wright DW. Hemozoin and antimalarial drug discovery. *Future Med Chem* (2013) **5**:1437–1450. doi:10.4155/fmc.13.113

51. Olivier M, Van Den Ham K, Shio MT, Kassa FA, Fougeray S. Malarial pigment hemozoin and the innate inflammatory response. *Front Immunol* (2014) **5**: doi:10.3389/fimmu.2014.00025

52. Dickinson-Copeland CM, Wilson NO, Liu M, Driss A, Salifu H, Adjei AA, Wilson M, Gyan B, Oduro D, Badu K, et al. Heme-mediated induction of CXCL10 and depletion of CD34+ progenitor cells is toll-like receptor 4 dependent. *PLoS One* (2015) **10**: doi:10.1371/journal.pone.0142328

53. Liu M, Wilson NO, Hibbert JM, Stiles JK. STAT3 Regulates MMP3 in Heme-Induced Endothelial Cell Apoptosis. *PLoS One* (2013) **8**: doi:10.1371/journal.pone.0071366

54. Armah HB, Wilson NO, Sarfo BY, Powell MD, Bond VC, Anderson W, Adjei AA, Gyasi RK, Tettey Y, Wiredu EK, et al. Cerebrospinal fluid and serum biomarkers of cerebral malaria mortality in Ghanaian children. *Malar J* (2007) **6**: doi:10.1186/1475-2875-6-147

55. Jain V, Armah HB, Tongren JE, Ned RM, Wilson NO, Crawford S, Joel PK, Singh MP, Nagpal AC, Dash AP, et al. Plasma IP-10, apoptotic and angiogenic factors associated with fatal cerebral malaria in India. *Malar J* (2008) **7**: doi:10.1186/1475-2875-7-83

56. Gui X, Yang H, Li T, Tan X, Shi P, Li M, Du F, Chen ZJ. Autophagy induction via STING trafficking is a primordial function of the cGAS pathway. *Nature* (2019) **567**:262–266. doi:10.1038/s41586-019-1006-9

57. Wu J, Chen YJ, Dobbs N, Sakai T, Liou J, Miner JJ, Yan N. STING-mediated disruption of calcium homeostasis chronically activates ER stress and primes T cell death. *J Exp Med* (2019) **216**:867–883. doi:10.1084/jem.20182192

58. Wan D, Jiang W, Hao J. Research Advances in How the cGAS-STING Pathway Controls the Cellular Inflammatory Response. *Front Immunol* (2020) **11**:615. doi:10.3389/fimmu.2020.00615

59. Couper KN, Barnes T, Hafalla JCR, Combes V, Ryffel B, Secher T, Grau GE, Riley EM, De Souza JB. Parasite-derived plasma microparticles contribute significantly to malaria infection-induced inflammation through potent macrophage stimulation. *PLoS Pathog* (2010) **6**: doi:10.1371/journal.ppat.1000744

60. Elphinstone RE, Riley F, Lin T, Higgins S, Dhabangi A, Musoke C, Cserti-Gazdewich C, Regan RF, Warren HS, Kain KC. Dysregulation of the haem-haemopexin axis is associated with severe malaria in a case-control study of Ugandan children. *Malar J* (2015) **14**:511. doi:10.1186/s12936-015-1028-1

61. Fortes GB, Alves LS, De Oliveira R, Dutra FF, Rodrigues D, Fernandez PL, Souto-Padron T, De Rosa MJ, Kelliher M, Golenbock D, et al. Heme induces programmed necrosis on macrophages through autocrine TNF and ROS production. *Blood* (2012) **119**:2368–2375. doi:10.1182/blood-2011-08-375303

62. Liu Y, Pal M, Bao W, Shi PA, Lobo CA, An X, Manwani D, Zhong H, Yazdanbakhsh K. Type I interferon is induced by hemolysis and drives antibody-mediated erythrophagocytosis in sickle cell disease. *Blood* (2021) **138**:1162–1171. doi:10.1182/blood.2021011629

63. Friedman JR, DiBenedetto JR, West M, Rowland AA, Voeltz GK. Endoplasmic reticulum-endosome contact increases as endosomes traffic and mature. *Mol Biol Cell* (2013) **24**:1030–1040. doi:10.1091/mbc.E12-10-0733

64. Takaoka A, Mitani Y, Suemori H, Sato M, Yokochi T, Noguchi S, Tanaka N, Taniguchi T. Cross talk between interferon-γ and -α/β signaling components in

caveolar membrane domains. *Science (80-)* (2000) **288**:2357–2360. doi:10.1126/science.288.5475.2357

65. Lienenklaus S, Cornitescu M, Ziętara N, Łyszkiewicz M, Gekara N, Jabłońska J, Edenhofer F, Rajewsky K, Bruder D, Hafner M, et al. Novel Reporter Mouse Reveals Constitutive and Inflammatory Expression of IFN-β In Vivo. *J Immunol* (2009) **183**:3229–3236. doi:10.4049/jimmunol.0804277

66. Tegtmeyer PK, Spanier J, Borst K, Becker J, Riedl A, Hirche C, Ghita L, Skerra J, Baumann K, Lienenklaus S, et al. STING induces early IFN-β in the liver and constrains myeloid cell-mediated dissemination of murine cytomegalovirus. *Nat Commun* (2019) **10**: doi:10.1038/s41467-019-10863-0

67. Adachi O, Kawai T, Takeda K, Matsumoto M, Tsutsui H, Sakagami M, Nakanishi K, Akira S. Targeted disruption of the MyD88 gene results in loss of IL-1- and IL- 18-mediated function. *Immunity* (1998) **9**:143–150. doi:10.1016/S1074-7613(00)80596-8

Legends to the Figures

Figure 1. Brain pathology and cerebral malaria lethality associated to type I IFN responses in malaria infection. (A) Interferon response signature detected in the in the designated brain regions was evaluated by measuring interferon-stimulated gene expression by quantitative PCR (qPCR). Data points represent individual mice (n=10) from two independent infection experiments. Symptomatic *Pba*-infected mice (day 6 PI) were compared to non-infected mice using unpaired, two-tailed *t*-test, Mann Whitney test (p values on the figure). (B) *Ifnβ1* gene expression in the indicated organs of IFNβ-Luc reporter (IFNβ$^{+/\Delta\beta\text{-luc}}$) mice infected with *Pba* (day 6 PI) or non-infected was ascertained by *ex vivo* luciferase activity normalized for tissue protein contents. Data points represent individual mice from one representative experiment out of three performed. Data was compared with one-way ANOVA using Tukey's multiple comparisons test. (C) Brain blood barrier integrity was evaluated by Evans Blue (EB) quantification in the brain after mouse perfusion. Data were normalized for brain weight in wild type and IFNβ KO mice at day 6 PI. Experimental groups were compared by one-way ANOVA, Tukey's multiple comparisons test (n=6 or n=3 for NI IFNβ KO mice). (D) Survival curve of wild type and IFNβ KO mice infected with 10^6 *Pba*-IE. Dashed line delimits the time-window of death by CM. Data comprising two independent infection experiments and compared with Gehan-Breslow-Wilcoxon test.

Figure 2. Analysis of innate sensing mechanisms for type I IFN induction reveals STING1 contribution to brain IFNβ response and cerebral malaria lethality. Survival and blood parasitemia curves in mice deficient for TLR signaling molecules (MyD88 and TRIF KO mice) (A) or in RNA/DNA sensing molecules (MDA5, MAVS

and STING1 KO mice) (B). Data for each KO strain comprise two independent infection experiments. Gehan-Breslow-Wilcoxon test was applied to compare survival curves of wild type and KO infected mice. (C) Induction of *Ifnβ1* gene expression in the indicated organs of IFNβ-Luc reporter (IFNβ$^{+/\Delta\beta\text{-luc}}$STING1$^{+/-}$) and in IFNβ-Luc reporter lacking STING (IFNβ$^{+/\Delta\beta\text{-luc}}$STING1$^{-/-}$) mice infected with *Pba* (day 6 PI) was ascertained by *ex vivo* luciferase activity normalized for tissue protein amounts. Data was compared between infected animals with one-way ANOVA using Tukey's multiple comparisons test.

Figure 3. Leukocyte brain infiltration is mediated by STING1 induction of *Ifnβ* and *Cxcl10* in the brain. (A) *Ifnβ1* gene expression in the brain of mice with two reporter alleles for *Ifnβ1* (IFNβ$^{\Delta\beta\text{-luc}/\Delta\beta\text{-luc}}$) at day 4 of infection was ascertained by *ex vivo* luciferase activity normalized for tissue protein amounts. (B) *Cxcl10* gene expression (qPCR) in the brain of wild type and IFNβ and STING1 KO mice at day 4 of infection. Unpaired, two-tailed *t*-test, Mann Whitney test. (C) Representative flow cytometry dot blots showing the percentage of CD45^{high} cells within brain infiltrates of wild type and STING1 KO mice.

(D) Flow cytometry analysis of brain leukocytes isolated from non-infected or *Pba*-infected (day 6 PI) wild type and STING1 KO mice. Extracellular staining against CD45 in combination with staining for TCRβ, CD8 and Mac-1 identified CD8+T cells (CD45^{+} TCRβ^{+} CD8^{+}), monocytes (CD45^{high} Mac-1^{+}), and microglia (CD45^{int}Mac-1^{+}). Activated CD8^{+}T cells were identified by extracellular expression of CD62L and CD44 and intracellular staining for Granzyme B and IFNγ. MHC I expression identified

activated microglial cells. Experimental groups were compared using one-way ANOVA with Tukey's multiple comparisons test (****p<0.0001)

Figure 4. **STING1 expression on brain endothelial cells is a determinant of IFNβ induction and CM lethality**. *Ifnβ1* gene expression was ascertained by *ex vivo* luciferase activity in mice infected with *Pba* (day 6 PI) and non-infected mice carrying a IFNβ-Luc reporter conditionally activated in cells expressing (A) GFAP (glial cells), (B) LysM (myeloid cells), (C) CX3CR1 (microglia cells) (D) Tie-2 (endothelial and hematopoietic cells) or (E) Slco1c1 (brain endothelial cells). I.p. injection of Poly I:C was used as positive response control of *Ifnβ1* gene induction. Results comprise two independent infection experiments. Unpaired, two-tailed *t*-test, Mann Whitney test.

Survival curves after *Plasmodium* infection in mice carrying conditional or induced STING deletion driven by (F) CX3CR1Cre and CX3CR1CreERT (monocytes/microglia), (G) Tie2Cre (endothelial cells) or (H) Slco1c1CreERT (brain endothelial). Results represent at least three independent infection experiments for each mouse strain. Gehan-Breslow-Wilcoxon test.

Figure 5. MPs isolated from blood and EPs induce IFNβ in brain endothelial cells after acidic processing and in a STING1-dependent manner. (A) NanoSight analysis of mean particle size after serum centrifugation (20 000g) of symptomatic *Pba*-infected mice (day 6 PI) and non-infected control mice. Results represent two independent infection experiments. Non-infected mice were compared with *Pba*-infected mice by unpaired, two-tailed *t*-test, Mann Whitney test. (B) TEM image of negative stained MPs obtained from the serum of mice with CM or non-infected animals. (C) Representative

flow cytometry histograms of serum MPs stained with the indicated cell lineage membrane markers. MPs were collected after 20 000g centrifugation from non-infected (full histogram) and infected (empty histogram) mice. Data shown are representative of three independent experiments. (D) *Ifnβ1* RNA quantification in BECs stimulated with MPs isolated from the serum (600 µl) of symptomatic *Pba*-infected mice (day 6 PI) (MPs-CM, n=6 independent isolation experiments) and non-infected control mice (MPs-NI, n=3 independent isolation experiments). Exposure to LPS (1 µg/ml) and Poly I:C (5 µg/ml) were used as positive response controls. Treated cells were compared to control (CTR) non-treated cells by one-way ANOVA. (E) Measurement of luciferase activity in IFNβ-reporter BECs exposed to two different doses ($2x10^5$ and $2x10^6$) of erythrocytes isolated from the blood of non-infected (NIE) or *Pba*-infected mice (IE), or with EPs obtained from IE-cultures centrifuged at 20 000g. Data are representative of two experiments and compared with one-way ANOVA using Tukey's multiple comparisons test. (F) Activation of *Ifnβ1* gene expression measured by luciferase activity in IFNβ-reporter BECs treated or not with NH4CL (20 mM) and then exposed to EPs collected from *Pba*-IE cell cultures. One representative experiment of three performed in triplicate is shown. Data was compared with one-way ANOVA using Tukey's multiple comparisons test. (G) *Ifnβ1* gene expression measured by luciferase activity in IFNβ-reporter WT or STING1 KO BECs stimulated with EPs. Results comprise data of two independent experiments. Treatments are compared between the two genotypes by two-way ANOVA using Tukey's multiple comparisons test.

Fig. 6. Heme sequestered by the parasite induce *Ifnβ1* and *Cxcl10* gene expression in BECs through STING1 activation. (A) Flow cytometry analysis of EPs staining for TER119 and/or GFP-positive. Data comprising four independent experiments were

compared to Fr1 by two-way ANOVA, Dunnett's multiple comparisons test. ****p<0.0001, **p<0.01. (B) TEM imaging of Fr2 (fixed sample) showing membrane structures surrounding hemozoin crsytals. (C) Measurement of luciferase activity in IFNβ-reporter BECs stimulated with each of 5 different EPs fractions (see Fig. S5A); $2x10^5$ EPs/fraction. Data comprise two (Fr4), four (Fr1 and Fr3), six (Fr5) and ten (Fr2) independent isolation experiments and each spot represents a cell culture well. One-way ANOVA, Tukey's multiple comparisons test. (D) *Cxcl10* gene expression in BECs stimulated with blood of *Pba*-infected mice containing $2X10^5$ IE and with $2x10^5$ EPs of different fractions. Data comprise 3-4 experiments of different BECs and EPs isolations and are compared between genotypes by two-way ANOVA using Tukey's multiple comparisons test, *p<0.05, **** p<0.0001. Each spot represents a cell culture well. (E) Luciferase activity in IFNβ-reporter BECs exposed to $2x10^6$ EPs from *Pba*-IE cultured presence or absence of chloroquine (8 μM). Results are from one representative experiment of two performed in triplicate and were compared to CTR cells by one-way ANOVA, Tukey's multiple comparisons test. (F) Luciferase activity in IFNβ-reporter BECs stimulated with Hemin or Hemozoin at the indicated concentrations or with IFNβ (1,000 U/ml). Data comprise 2-3 independent experiments and each point represents a cell culture well. Comparison to CTR cells were performed by one-way ANOVA, Tukey's multiple comparisons test. (G) *Cxcl10* gene expression in wild type or STING1 KO BECs stimulated with different concentrations of hemin for 20h. Data comprise two independent experiments. Comparison between genotypes were performed by two-way ANOVA, Tukey's multiple comparisons test, * p<0.05. (H) STING1-Heme molecular docking results. Close-up view of STING1 pocket with superposition of best-scoring docked pose of c-di-GMP and Heme. c-di-GMP and Heme are colored in yellow and cyan sticks, respectively. Molecular docking was performed using GOLD software and

ChemPLP as scoring function. (I) Detection of peroxidase activity and migration shift assay of STING1 (1μM) incubated with increasing doses of heme. Albumin (5 μM) incubated with heme and heme alone were used as positive and negative controls of peroxidase activity, respectively.

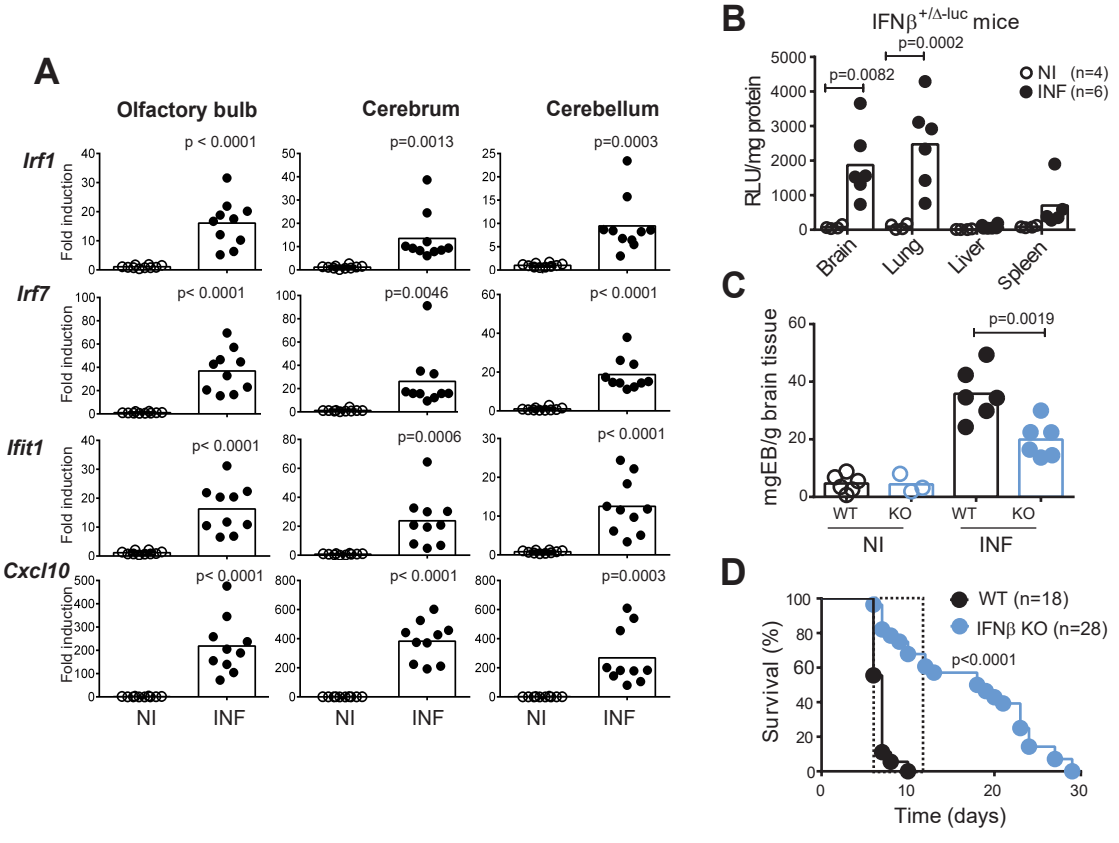

Fig. 1, Pais et al

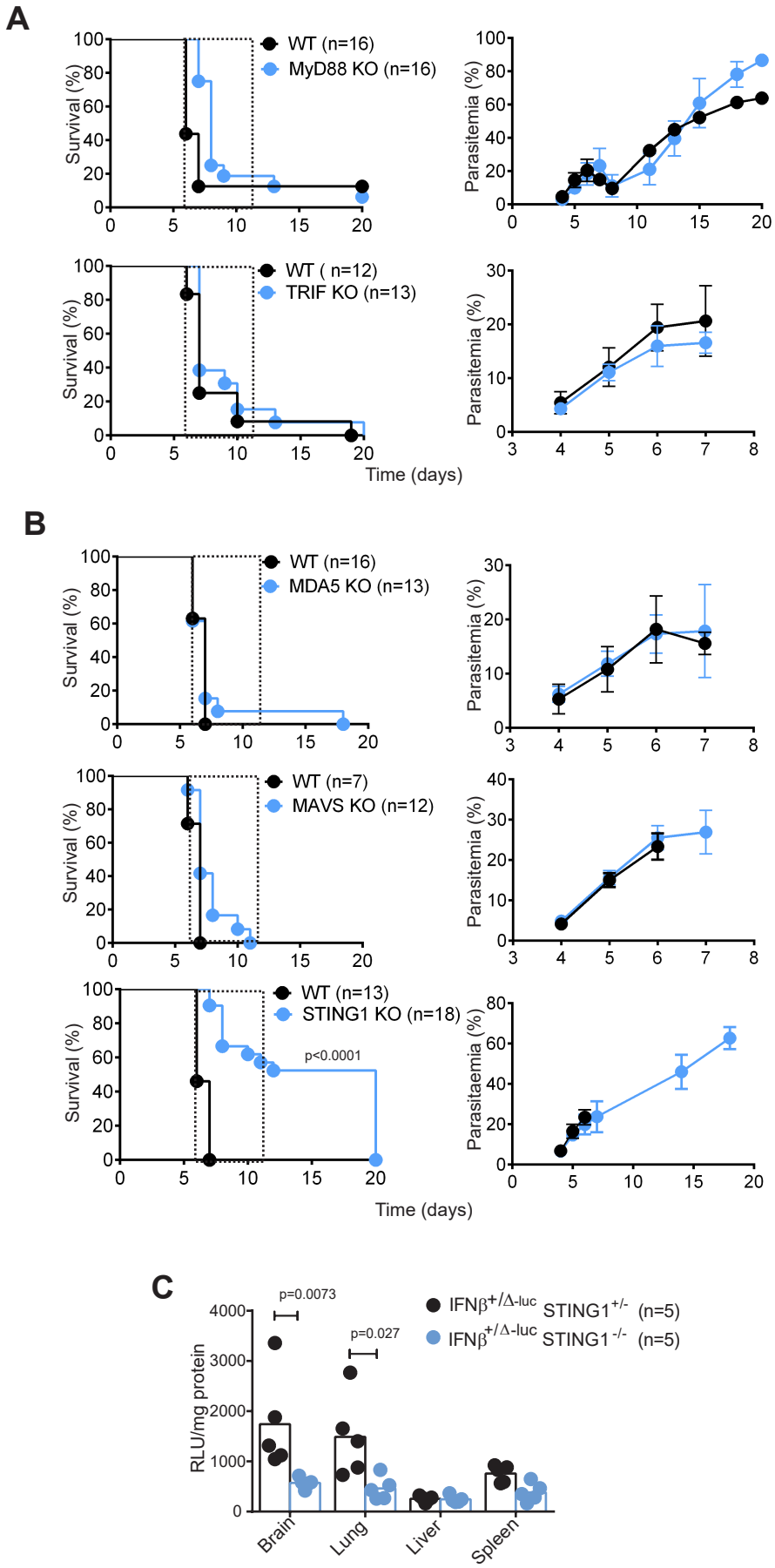

Fig. 2, Pais et al

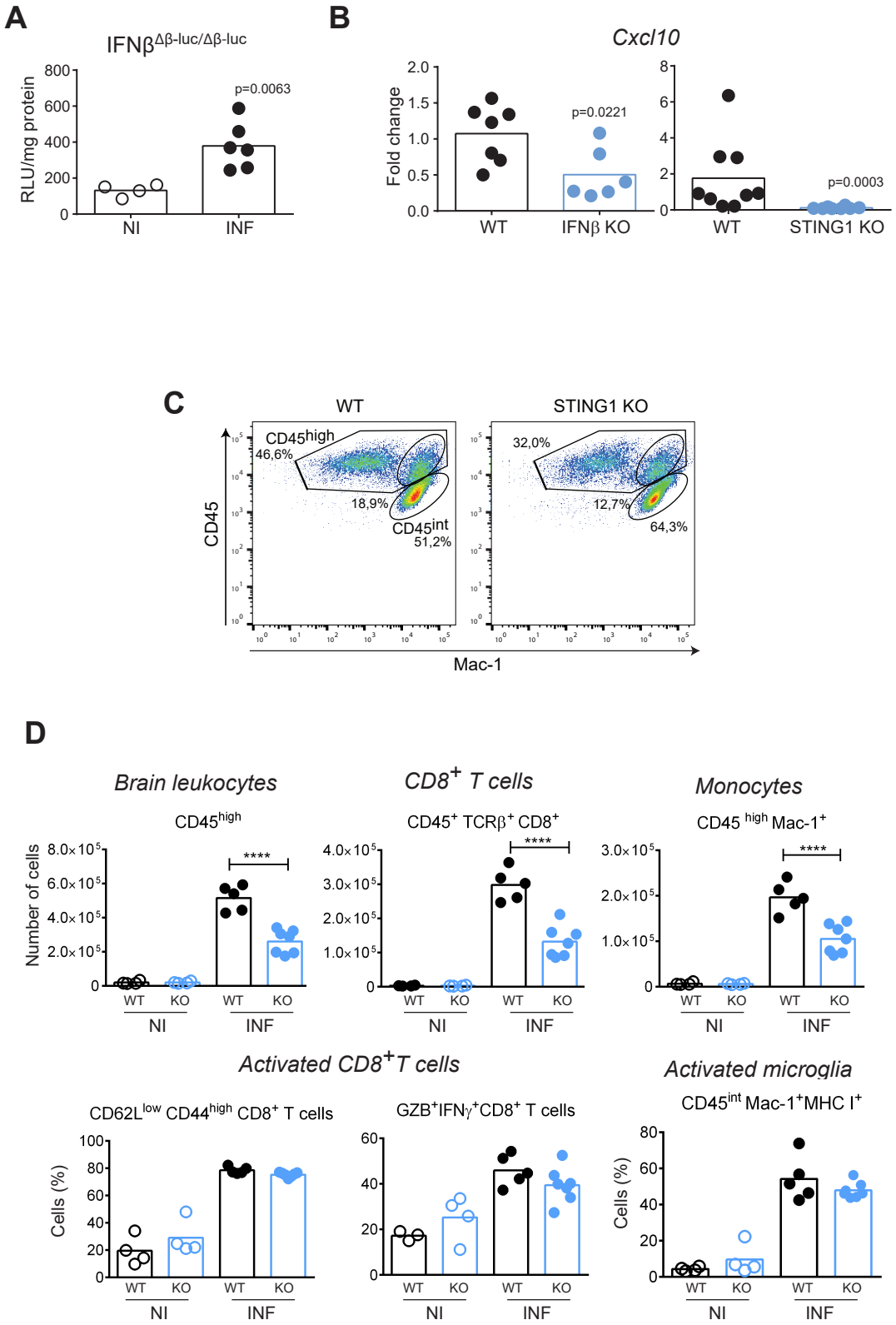

Fig. 3, Pais et al

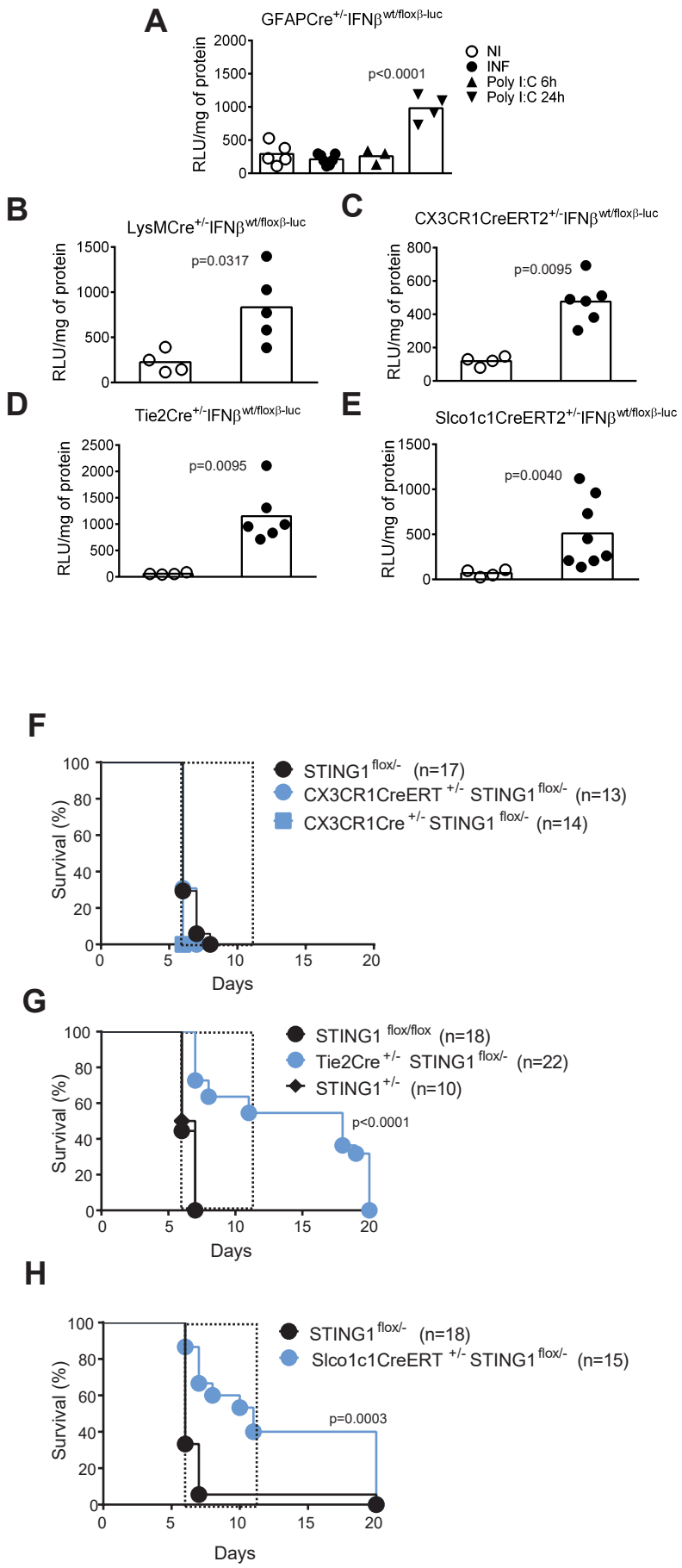

Fig. 4, Pais et al

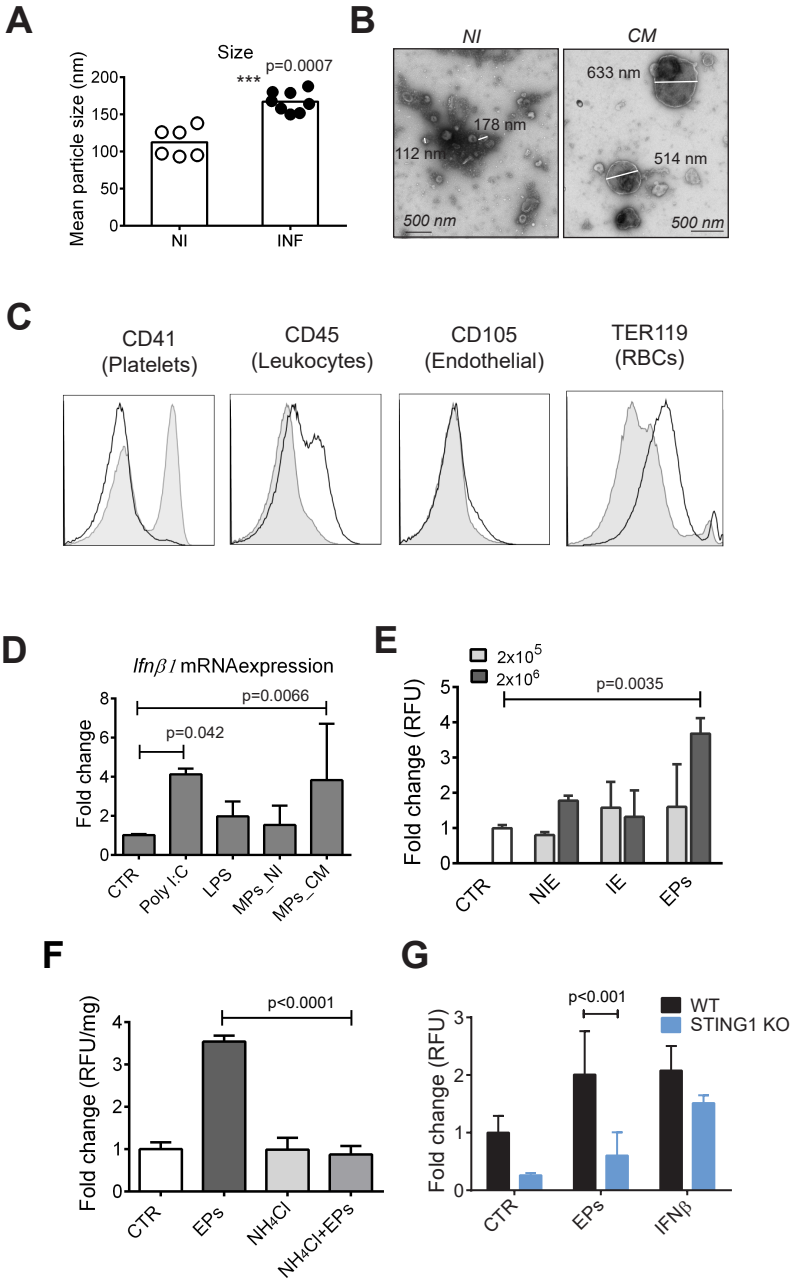

Fig. 5, Pais et al

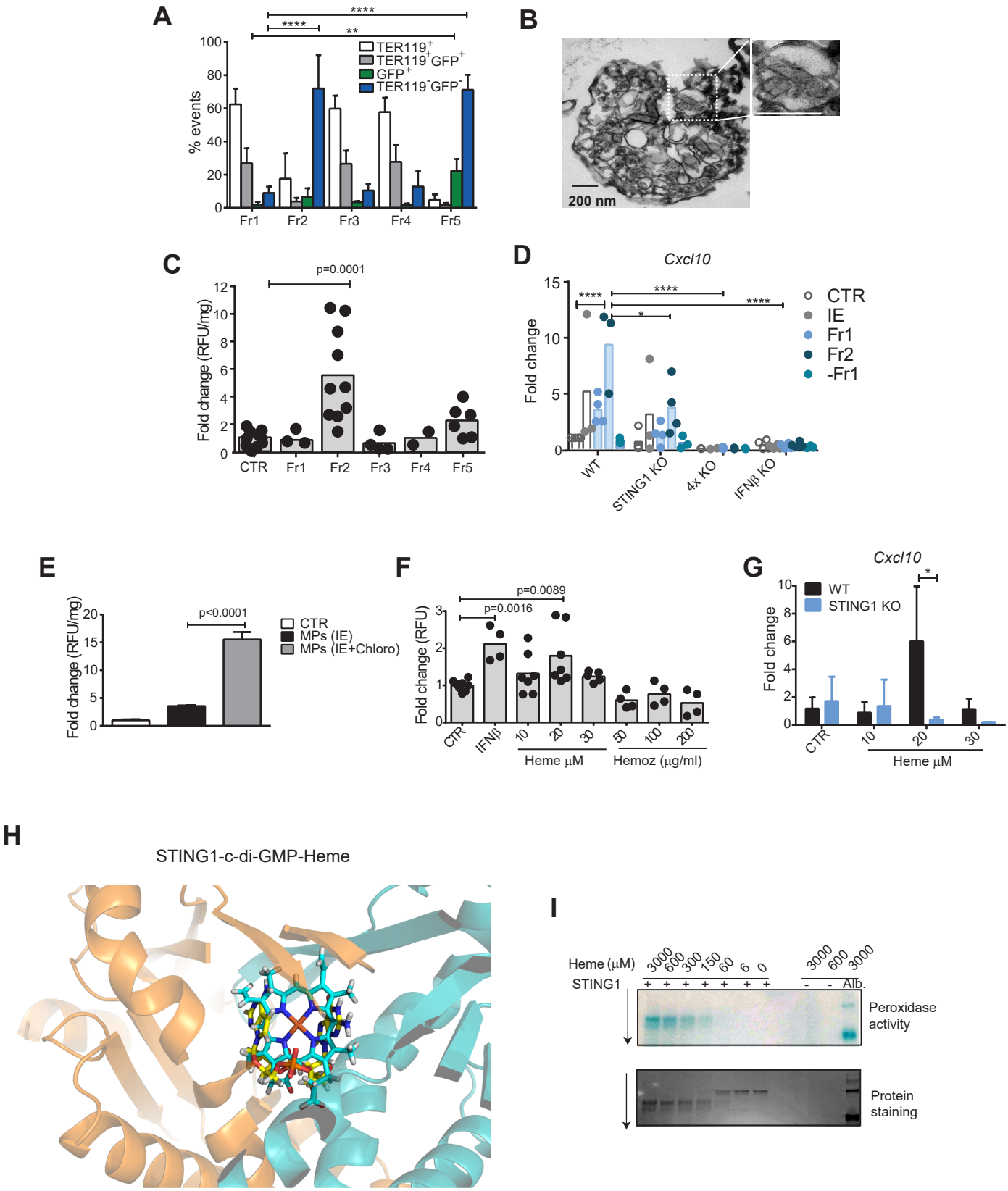

Fig. 6, Pais et al